HHS Public Access

Author manuscript

Nat Med. Author manuscript; available in PMC 2011 June 01.

Published in final edited form as:

Nat Med. 2010 December ; 16(12): 1444–1449. doi:10.1038/nm.2260.

Noninvasive multi–photon fluorescence microscopy resolves retinol and retinal–condensation products in mouse eyes

Grazyna Palczewska[1], **Tadao Maeda**[2,3], **Yoshikazu Imanishi**[3], **Wenyu Sun**[1], **Yu Chen**[3], **David R. Williams**[4], **David Piston**[5], **Akiko Maeda**[2,3], and **Krzysztof Palczewski**[1,3]

[1] Polgenix Inc., Cleveland, Ohio 44106, USA

[2] Department of Ophthalmology and Visual Sciences, Case Western Reserve University, Cleveland, USA

[3] Department of Pharmacology, Case Western Reserve University, Cleveland, Ohio, USA

[4] Center for Visual Science, University of Rochester, Rochester, New York, USA

[5] Department of Molecular Physiology and Biophysics, Vanderbilt University, Nashville, Tennessee, USA

Abstract

Multi–photon excitation fluorescence microscopy (MPM) can image certain molecular processes *in vivo*. In the eye, fluorescent retinyl esters in sub–cellular structures called retinosomes mediate regeneration of the visual chromophore, 11–*cis*–retinal, by the visual cycle. But harmful fluorescent condensation products were also identified previously. We report that in wild type mice, excitation with λ ~730 nm identified retinosomes in the retinal pigment epithelium, whereas excitation with λ ~910 nm revealed at least one additional retinal fluorophore. The latter fluorescence was absent in eyes of genetically modified mice lacking a functional visual cycle, but accentuated in eyes of older WT mice and mice with defective clearance of all–*trans*–retinal, an intermediate in the visual cycle. MPM, a noninvasive imaging modality that facilitates concurrent monitoring of retinosomes along with potentially harmful products in aging eyes, has the potential to detect early molecular changes due to age–related macular degeneration and other defects in retinoid metabolism.

Correspondence to: Krzysztof Palczewski (kxp65@case.edu) or Grazyna Palczewska (gpalczewska@polgenixinc.com).

Contributions

G.P. and K.P. conceived and directed the project. G.P., T.M., Y.M., W.S., Y.C. and A.M. designed and conducted experiments. G.P. and K.P. prepared the manuscript. Y.M., D.W.P. analyzed the data and edited the manuscript, D.R.W. edited the manuscript.

Competing financial interests

G.P. and W.S. are employees of Polgenix. K.P. is CSO at Polgenix Inc. K.P. and Y.M. are inventors of the U.S. Patent No. 7,706,863 whose value may be affected by this publication. T.M., Y.C., D.W.P. and A.M. report no conflict of interests. D.R.W. laboratory received support from Polgenix Inc.

Keywords

Photoreceptor cells; fluorescence microscopy; retinosomes; retinyl esters; A2E; RPE; retina; two–photon fluorescence excitation microscopy; three–photon fluorescence excitation microscopy

High resolution noninvasive imaging has become an essential method for understanding complex biological systems in experimental cell lines and is used with increasing frequency in tissues and live animals [1–5]. These methods are also being slowly adapted for diagnostic testing and clinical applications where they show great promise [2,6,7]. Two–photon microscopy (TPM) offers real time, high–resolution images of endogenous fluorescent molecules in living tissues with little or no tissue damage [8–11]. Use of long–wavelength and non–linear excitation bypasses absorption by UV and visible light chromophores and allows imaging at low laser power with sub–cellular resolution at tissue depths not attainable with other noninvasive optical modalities. Vertebrate eyes have evolved to prevent short UV wavelength light from reaching the retina. Instead, infrared illumination used in multi–photon microscopy is ideal for visualizing fluorescent biomarkers that exist endogenously in retinal pigment epithelial (RPE) cells of the eye.

There are two types of fluorescent retinoids indicative of certain functional and disease states of human eyes. The intrinsic chromophore, fatty–acid esterified retinol, displays weak fluorescence and has a propensity to cluster with phospholipids and helper proteins into structures called retinosomes located close to the RPE plasma membrane [12–14]. Fatty acid–esterified retinol is generated by sequential reactions of the visual cycle (Supplementary Fig. 1). First, photoisomerization of 11–*cis*–retinylidene, the light sensitive chromophore of visual pigments in rods and cones, generates all–*trans*–retinylidene, which then is hydrolyzed and reduced to retinol. Next, retinol is transported from photoreceptors to the RPE and esterified in a LRAT–dependent reaction; additionally, these esters are formed from retinol imported from the circulation [15]. As demonstrated by noninvasive *in vivo* TPM imaging through the sclera, and by chemical analyses of eyes of wild–type (WT) and genetically modified mice, retinosomes accumulate fatty acid–esterified retinol essential for 11–*cis*–retinal production. Thus, retinosomes serve as the reservoir of all–t*ran*s–retinyl esters for dynamic transfer and conversion of retinoids in the eye.

Condensation products of all–*trans*–retinal are also fluorescent and their accumulation within the RPE is indicative of aging retina or retinal pathology. These stable condensation products, including A2E, A2DHP–PE and all–*trans*–retinal dimers [16] that result from inadequate clearance and conversion of all–*trans*–retinal back to 11–*cis*–retinol through the visual cycle [17,18], comprise the lipofuscin of RPE. All–*trans*–retinal itself is a reactive cytotoxic aldehyde that can damage the retina [17,18], but the relative toxicities of its condensation products have not been fully clarified. Several explanations for such toxicity have been proposed including complement activation [19,20], destruction of membrane structures [16], and photo–oxidative damage by acting as a chromophore for blue light [21]. Retinyl esters and all–*trans*–retinal condensation products must be spectrally resolved to monitor their status independently.

Herein we describe studies that extend the use of noninvasive multi–photon fluorescence microscopy to the study of native tissues within the eye. Spectral analyses of fluorophores activated at two different wavelengths and chemical analyses of the eyes in mice with different genetic backgrounds revealed distinguishing features between retinosomes and condensation products of all–*trans*–retinal associated with retinal pathology. Imaging methods described herein could be highly useful to assess the outcome of pharmacological interventions.

RESULTS

Fluorescent images of the RPE excited by an infrared femtosecond laser

Consistent with published results [12–14], we identified retinosomes in the RPE of mice by using a 730 nm femptosecond (fs) laser (Fig. 1a). The emission spectrum analyzed from fluorescence obtained from the area outlined by the yellow rectangle in Fig. 1a displayed two maxima at 480 nm and 521 nm (Fig. 1b). This spectrum was super–imposable with that of authentic all–*trans*–retinol solution in ethanol obtained under identical experimental conditions (Supplementary Fig. 2a). The two–photon spectra differed from those derived from UV excitation of retinol that produced a much stronger emission at 480 nm, as compared to the 521 nm peak which only appeared as a shoulder. This difference likely resulted from a complex electron excitation/relaxation structure for this conjugated polyene, wherein the lower energy component is enhanced by two–photon excitation. Retinol also emits at longer excitation wavelengths (Supplementary Fig. 2a), so we analyzed the RPE with an excitation wavelength of 910 nm (Fig. 1c). While a strong fluorescence was observed, it differed from that of retinosomes by having a maximal emission at ~570 nm (Fig. 1b), suggesting the presence of fluorophores other than retinol within the RPE. We also observed a very strong second harmonic (SH) signal derived from the sclera (Fig. 1c, blue box, and Fig. 1b, SH) that likely originates from collagen enriched structures [9]. Fluorescence emission spectra were the same whether images were obtained directly from flat–mounted RPE, or through the sclera of the intact eye (Fig. 1b; image in Fig. 1d).

Images taken as a function of excitation wavelengths with constant laser power and detector setting revealed that the high fluorescence emission observed at 720 nm excitation decreased until 850 nm and then increased again at 910 nm (Fig. 2a). However, the well–defined fluorescent pattern of retinosomes obtained with 730 nm excitation (Fig. 2b) was replaced with more uniformly distributed cellular structures at the longer 910 nm excitation wavelength (Fig. 2c). Moreover, the spectrum systematically shifted from a shorter– to a longer–wavelength emission as the excitation wavelength increased from 720 nm to 910 nm (Supplementary Fig. 2b).

Visualization of retinosomes by three–photon excitation spectroscopy

If the unidentified fluorophores emitting in response to 910 nm excitation were condensation products of all–*trans*–retinal produced from bleached visual pigments [16], they should be absent in Rpe65 knockout mice that have a defective visual cycle [22]. Fluorescence as a function of increasing excitation light wavelength in these mice exhibited a monotonic decay with no increase in signal observed at 910 nm (Fig. 3a, Supplementary Fig. 3).

Excitation at either 730 nm or 910 nm elicited the same emission spectrum, suggesting that retinyl esters are visualized with both 730 nm and 910 nm excitation. Moreover, the emission spectrum was consistent with those derived from WT mice with 730 nm excitation (Fig. 3b). Identification of retinosomes in *Rpe65*$^{-/-}$ mice was further confirmed by gavaging these animals with artificial chromophore [23,24]. Expansion of retinosomes and increased retinyl ester content after these mice were treated with 9–*cis*–retinyl acetate was apparent (Supplementary Fig. 4).

All–*trans*–retinyl esters or retinol exhibit a maximal emission at ~480 nm with a shoulder at longer wavelengths when examined in a mixture of organic solvents (Supplementary Fig. 5a) [25]. Fluorescence of retinosomes in retinas of *Rpe65*$^{-/-}$ mice subjected to two–photon excitation with 910 nm should be negligible, given that the optical density of retinol (or retinyl esters) at half this wavelength, i.e. 455 nm, is only 0.3% of that at 365 nm (half of 730 nm) with single–photon excitation in hexane (Supplementary Fig. 5b). Moreover, the optical density at 303 nm for retinol should be 64% of its maximal absorption at 326 nm, thus, it is more likely that the 910 nm–induced signal is the result of three–photon excitation. Accordingly, we found that retinyl esters are indeed excited by simultaneous absorption of three 910 nm photons. The probability of excitation by three–photon excitation is proportional to light intensity cubed (light intensity^3), whereas the probability by two–photon excitation is proportional to the light intensity squared (light intensity^2). At an excitation wavelength of 910 nm, fluorescence emission was proportional to the 2.83rd power of the excitation intensity (Fig. 3c), indicating a significant contribution of the three–photon effect. The third power dependence, rather than the second power dependence, showed good agreement with the data. At a control excitation wavelength of 730 nm, fluorescence was found to be proportional to the 2.12th power (Fig. 3d), consistent with a two–photon effect.

Abca4$^{-/-}$Rdh8$^{-/-}$ mice accumulate high levels of A2E

Abca4$^{-/-}$*Rdh8*$^{-/-}$ mice exhibit both deficient transport of all–*trans*–retinal from the internal discs and a reduced capacity for all–*trans*–retinal reduction and clearance [18,26,27]. Consequently, they accumulate large amounts of A2E and other all–*trans*–retinal condensation products. Images obtained with wavelengths of excitation light that increased from 720 nm to 910 nm were consistently brighter than those from WT mice (Fig. 4a), with exceptionally high fluorescence seen at 910 nm. Spectra with 730 nm excitation displayed the characteristic retinol/retinyl ester emission peak together with a peak at about 560 nm attributable to retinal condensation products (Fig. 4b). As expected, the contribution of retinosomes to this emission spectrum was reduced. Importantly, the bright fluorescence, though punctate, was spread throughout cells (Fig. 4c,d) at all wavelengths tested (Fig. 4c). Synthetic A2E standard had a similar emission spectrum with maximum shifted to the longer wavelength when examined by two–photon excitation (Supplementary Fig. 2a), an observation similar to previous findings [28]. These results and those obtained with WT, *Lrat*$^{-/-}$ and *Rpe65*$^{-/-}$ mice (Supplementary Fig. 6) strongly correlate with levels of all–*trans*–retinyl esters and A2E found in the retinas of these mice (Fig. 5). Because A2E accumulates with age, images obtained with excitation wavelengths of 730 nm and 910 nm could be extremely helpful in discriminating between essential retinoids of the visual cycle,

such as retinols and retinyl esters present in retinosomes, and potentially harmful retinoids such as excessive amounts of all–*trans*–retinal and its condensation products.

Two–photon imaging to detect retinal aging

To test the ability of TPM to detect retinal aging, fluorescence images were obtained from WT mice at different ages and excitation wavelengths (Fig. 5a). Fluorescence emission decreased drastically with increasing excitation wavelengths in 7–week–old mice, but in 23–week–old mice fluorescence emission at longer wavelengths was elevated. Therefore, we systematically evaluated ratios of fluorescence obtained with 910 nm excitation to the fluorescence with 730 nm excitation and plotted these ratios as a function of age (Fig. 5b). As expected, WT mice exhibited an increase in these ratios as a function of age, presumably because A2E and other all–*trans*–retinal condensation products accumulated. Moreover, 14–week–old control *Abca4*$^{-/-}$ *Rdh8*$^{-/-}$ mice with significantly elevated A2E evidenced a very high 910 nm/730 nm fluorescence ratio whereas 17–week–old *Rpe65*$^{-/-}$ mice that do not produce A2E had a very low ratio [22], even below that exhibited by young WT mice. We then tested the level of retinyl esters as a function of age and found that this retinoid accumulates with age as previously observed (Fig. 5c) [24]. Importantly, A2E increased with age as well (Fig. 5d). In the presence of both A2E and all–*trans*–retinyl esters in WT and *Abca4*$^{-/-}$*Rdh8*$^{-/-}$ mice, we observed much more fluorescence from A2E, because excitation of A2E appears to be more efficient at the longer wavelengths than the three–photon excitation of retinyl esters. This was manifested by increased levels of fluorescence at longer wavelengths. At longer excitation wavelengths the two–photon emission spectrum of lipofuscin in human RPE overlaps the spectrum of WT mouse RPE (Supplementary Fig. 7).

DISCUSSION

The aims of this study were to: i) optimize multi–photon imaging of retinosomes; ii) use multi–photon spectroscopy to distinguish among retinal fluorophores; and iii) examine the use of noninvasive multi–photon spectroscopy to monitor changes in the retina caused by inherited visual disorders and aging.

Our study reveals that auto–fluorescent images of the retina, specifically the RPE, can be obtained at two excitation wavelengths, namely one at ~730 nm and the other at ~910 nm. Excitation with ~ 730 nm photons clearly images retinosomes in the two–photon mode, whereas ~910 nm photons primarily excite fluorophores related to the condensation of all–*trans*–retinal, e.g. A2E, A2DHP–PE and retinal dimers [16]. Only under special circumstances can retinosomes be imaged with ~910 nm photons, as in *Rpe65*$^{-/-}$ mice where they are enlarged. In such cases, nearly simultaneous absorption of two– and even three photons can take place. These findings are consistent with maximal absorption of all–*trans*–retinyl esters or all–*trans*–retinol at 326 nm (Supplementary Fig. 5), and A2E at ~440 nm [16]. There are several differences between retinosomes and retinoid–condensation products: i) retinosomes are located close to the plasma membrane and surrounded by adipose differentiation–related protein [12], whereas condensation products are spread throughout the cell; ii) each displays a fluorescence emission spectrum unique to its chemical and cellular structures; and iii) all–

trans–retinal condensation products not only accumulate with age but they also are either highly elevated or absent in mice with certain deletions of genes encoding enzymes of the visual cycle. Condensation products are proposed to be generated in photoreceptors and accumulated in lysosomes of the RPE, and the distribution of condensation products observed here (Figs. 2, 4) fits this description [13].

In the RPE, levels of all–*trans*–retinal condensation products increase with age [16] because each day about 10% of our rod outer segments, where these products are formed, are shed and phagocytosed by RPE cells [29]. These conjugates accumulate within the RPE because their breakdown is either slow or non–existent in mammals. Even though fluorescent retinosomes were clearly observed in mice when fluorescence was measured upon excitation at 730 nm and 910 nm, emission from condensation products dominated upon 910 nm excitation. Thus, it appears that the emission fluorescence ratio after excitation at these two wavelengths, i.e. the 910 nm/730 nm ratio, might be used to monitor the health of the retina and evaluate the efficacy of therapeutic agents, at least in mice.

The total background autofluorescence of the fundus examined by scanning laser ophthalmoscopy (SLO) at the same laser power (sensitivity at 100) also reflected the amounts of A2E in mice (Supplementary Fig. 8, Fig. 5d). However, because adjustments in laser power are required for each individual to compensate for different eye conditions such as cataracts, direct comparison of SLO values between individuals and time points poses potential problems. Moreover, the infrared laser of current SLO cannot cause two–photon excitation. Therefore, the 910 nm/730 nm excitation ratio of TPM offers a greater advantage in assessing the health of the retina.

TPM provides several advantages over single photon microscopy in monitoring the human eye. The human lens and macular pigments are highly opaque to UV and blue light, respectively. Therefore, it is especially difficult to deliver excitation light safely and efficiently to UV–blue absorbing fluorophores existing in the macula. Instead of using short wavelength excitation, TPM takes advantage of infrared illumination to excite UV–blue absorbing fluorophores such as retinyl esters and A2E, whose dynamics and quantities change in the macula of pre–AMD patients. In AMD, increasing RPE fluorescence is one of the earliest changes observed [30]. A recent large–scale prospective study of patients with geographic atrophy (GA) showed that fundus autofluorescence at the margins of GA was the best predictor of GA progression. The unique ability of our TPM to simultaneously image intermediates and byproducts of the visual cycle in the intact eye, enables monitoring formation of all–*trans*–retinal condensation products *in vivo* by comparing the ratio of fluorescence excited with 730 nm to 910 nm. Moreover, as observed by us and others, all–*trans*–retinal levels required to produce toxicity in vitro (5 μM) are also found *in vivo*, especially after bright light exposure. A lifetime of light exposure has been proposed as one of several risk factors for advanced AMD [18,31].

Other advantages of TPM include less light scattering with resultant deeper penetration, intrinsic three–dimensionality and a decreased risk of photobleaching and phototoxicity. TPM is also a growing technology with potential applications to both basic science and clinical research [32]. However most current TMP applications employ exogenous fluorescent

markers rather than endogenous fluorophores and most other procedures involving larger organisms are invasive.

By taking advantage of an animal model for Leber congenital amaurosis (the *Rpe65*$^{-/-}$ mouse) we quantitatively determined that three–photon microscopy can generate a fluorescent image characteristic of this disease. Three–photon microscopy requires three photons to be absorbed per fluorescent event and the excitation is proportional to the instantaneous intensity of incident laser light (*I*) to the third power. If imaging conditions are identical, the ratio of three–photon excited fluorescence to two–photon excited fluorescence is proportional to $\delta_3 \cdot I/\delta_2$, where δ_2 is the two–photon excitation cross section and δ_3 is the three–photon excitation cross section [11]. We are not aware of any data directly dealing with two or three–photon excitation cross sections as a function of wavelength for all–*trans*–retinyl esters, so we used existing data for retinol instead [33]. Based on several assumptions, we calculated whether three–photon excitation of retinyl esters might occur at 910 nm. We assumed that i) the two– and three–photon fluorescence quantum yields (η) are the same; and ii) the three–photon excitation cross section spectrum is offset from the two–photon excitation cross section spectrum by a factor of 10^{-33} [11], and that it parallels the two–photon excitation spectrum if the wavelengths are set to 3/2 times the corresponding two–photon process wavelengths. Then, using data for the wavelength-dependent two-photon fluorescence action cross section of retinol ($\eta \cdot \delta_2$), we estimate that at 910 nm $\eta \cdot \delta_2 \approx 8.8 \cdot 10^{-56}$ cm^{4}s per photon, and, taking into account that maximum absorption of retinol is at 326 nm (Supplementary Fig. 5), we estimate that three-photon cross section extrapolates to $\eta \cdot \delta_3$ $1.8 \cdot 10^{-86}$ cm^{6}s^2 per photon^2. Using these numbers and the intensity at 910 nm,

$$I_{910} \approx \frac{p_o \bullet \pi \bullet (NA)^2}{f_p \bullet \tau p \bullet h \bullet c \bullet \lambda} = 1.5 \bullet 10^{30} \text{ photons per cm}^2 s \quad \text{Equation 1}$$

where c is the speed of light, h is Planck's constant, NA is the numerical aperture, p_o is the average incident power, τ_p is the pulse duration, f_p is the pulse repetition frequency, and λ is the pulse center wavelength [34],we calculate that at 910 nm the ratio $\delta_3 \cdot I/\delta_2 \approx 0.3$. Following the same methodology but now at 730 nm, we calculated $I_{730} \approx 1.9 \cdot 10^{30}$ photons per cm^{2}s, $\eta \cdot \delta_2 \approx 3 \cdot 10^{-52}$ cm^{4}s per photon, $\eta \cdot \delta_3$ $9.2 \cdot 10^{-89}$ cm^{6}s^2 per photon^2 and $\delta_3 \cdot I/\delta_2 \approx 6 \cdot 10^{-7}$. These estimates suggest that three photon excitation of retinyl ester is feasible at 910 nm but not at 730 nm, supporting our experimental demonstration. Thus the three–photon effect has been demonstrated, perhaps for the first time, in a biological system, namely the intact, unfixed fresh eye.

In summary, TPM of endogenous fluorophores including retinyl esters, all–*trans*–retinol, and A2E provides a powerful way to monitor the visual cycle [15] directly and contribute to understanding the pathology of human retinal diseases. If we could visualize and understand early aberrations of these pathways in live human eyes, we would be better able to devise and monitor effective therapies for blinding retinal diseases.

METHODS

Mice

Lrat$^{-/-}$ and *Rpe65*$^{-/-}$ mice with a C57BL/6J background were crossed with C57 albino wild–type (WT) C57BL/6J–*Tyr*$^{C-2J}$ mice to produce albino *Lrat*$^{-/-}$ and *Rpe65*$^{-/-}$ animals. Albino *Abca4*$^{-/-}$*Rdh8*$^{-/-}$ double knockout mice were generated by crossing *Abca4*$^{-/-}$*Rdh8*$^{-/-}$ mice with a mixed 129Sv and C57BL/6J background with 129/SvJ albino WT mice [17,35]. PCR genotyping of these mice was performed as previously described [17,35–37]. Animals were housed and crossbred in the Case Western Reserve University (CWRU) Animal Resource Center Facility where they were maintained under either a 12 hr light (10 lux)/dark illumination cycle or in complete darkness. Manipulations in the dark were performed under dim red light transmitted through a filter (transmittance 560 nm; No. 1 Safelight; Eastman Kodak, Rochester, NY). Mice were provided free access to a standard chow diet and water. Prior to experimental analyses they were anesthetized by intraperitoneal injection with 10 μl/g body weight of 6 mg/ml ketamine and 0.44 mg/ml xylazine, and then euthanized by cervical dislocation. All animal procedures were approved by the CWRU Animal Care and Use Committee and complied with the American Veterinary Medical Association Guidelines on Euthanasia. Mice were gavaged with 9–*cis*–retinyl acetate according to a previously published protocol [38].

Retinoid and A2E Analyses

All experimental procedures related to extraction, derivatization, and separation of retinoids from dissected mouse eyes were carried out as previously described [17,35]. A2E was synthesized from all–*trans*–retinal and ethanolamine, and purified by HPLC [35]. Quantification of A2E after HPLC was accomplished by comparison with known concentrations of pure synthetic A2E standards [35].

Multi–photon excitation microscopy

TPM imaging was done with a Leica TCS SP2. A Ti:Sapphire laser (Coherent Chameleon XR) delivered <140 femtosecond (fs) laser pulses at 90 MHz. The excitation light was focused on samples by a Planapochromat 1.25 numerical aperture (NA), 0.1 mm working distance objective lens and fluorescence was collected through the same lens. Fluorescence intensities and cross-section images were obtained by offline analyses that employed Leica LCS Lite software, version 4.0 [39].

For imaging, a Hamamatsu R6357 photomultiplier tube was used as a non–descanned detector after filtering light through a band–pass Chroma filter, HQ 465/160. Before trans–scleral imaging and immediately after enucleation, a mouse eye was placed at the center of a glass bottomed 35–mm dish (MatTek Corporation, MA, USA), with the sclera contacting a coverslip and hydrated with solution of 9.5 mM sodium phosphate, pH 7.4, containing 137 mM NaCl and 2.7 mM KCl. The typical time between enucleation and data acquisition was less than 30 min. For flat–mount imaging, the cornea and lens were first dissected out of enucleated eyes with spring loaded scissors and the vitreous and retina were removed with tweezers. After four radial incisions, the RPE with choroid and sclera attached, was laid in

the center of a glass bottomed Matek dish and directly imaged with its apical side facing the glass.

Emission spectra were obtained with a Leica TCS SP2 spectrally sensitive detector in the descanned configuration. Regions of interest were outlined with Leica LCS Lite software version 4.0. Spectra were normalized to the maximum value for each sample. The z–position on the microscope was kept constant when imaging with variable wavelength excitation, taking into account that retinosome size is greater than 4 μm in the z direction as deduced from Fig. 1.

Characterization of fluorescence as a function of laser power

Imaging was done with 730 nm and 910 nm excitation wavelengths with 512×512 pixels/frame and 400 Hz line speed. Pixel size was 0.367 μm. Laser power was adjusted with a Leica TCS SP2 electro–optic modulator (EOM). At least 1 hr was allowed for the laser to stabilize and EOM to equilibrate with heat introduced by the infrared laser. Power was measured immediately before and after imaging in the sample plane with a calibrated Coherent FieldMax –TO laser power meter and a PM10 sensor. Laser power was measured by using the point bleach option with disabled scanning and blanking. To ensure that the laser beam was fully captured by the sensor, measurements employed a FL PLAN 0.25 NA objective with a 17.6 mm working distance. To determine if a two– or three–photon process was dominant we first assumed that (i) the two–photon excited fluorescence (N_{ex2}) is proportional to the incident laser power (p_0) squared and the two–photon fluorescence excitation cross section (δ_2) [10], $N_{ex2} \approx \delta_2 \cdot p_o^2$; (ii) and the three–photon excited fluorescence is proportional to the p_0 cubed and the three–photon fluorescence excitation cross section (δ_3) [40], $N_{ex3} \approx \delta_3 \cdot p_o^3$. Then the order of the process was determined from the slope of the line on the log–log plot.

Supplementary Material

Refer to Web version on PubMed Central for supplementary material.

Acknowledgments

We would like to thank M. Golczak for help during the course of this study and Z. Dong for expert handling of mice. We also thank LT Webster, and members of Palczewski's laboratory for critical comments on the manuscript. This research was supported in part by grants EY008061, EY009339, EY019880, EY019031, EY020715 and P30 EY11373 from the National Institutes of Health, TECH 09–004 from the State of Ohio Department of Development and Third Frontier Commission, ELSO – the European Life Scientist Organization and sponsored by the Klaus Tschira Foundation, Heidelberg, Germany.

Abbreviations used

A 2 E	2–[2,6–dimethyl–8–(2,6,6–trimethyl–1–cyclohexen–1–yl)–1*E*,3*E*,5*E*,7*E*–octatetraenyl]–1–(2–hydroxyethyl)–4–[4–methyl–6–(2,6,6–trimethyl–1–cyclohexen–1–yl)–1*E*,3*E*,5*E*–hexatrienyl]–pyridinium
ABCA4/ABCR	photoreceptor specific ATP–binding cassette transporter
AMD	age–related macular degeneration

fs	femtosecond
GA	geographic atrophy
LRAT	lecithin:retinol acyl transferase
MPM	Multi–photon excitation fluorescence microscopy
RPE65	retinoid isomerase
TFA	trifluoroacetic acid
TPM	two–photon microscopy
SLO	scanning laser ophthalmoscope
vitamin A	retinol
WT	wild type

References

1. Schenke-Layland K, Riemann I, Damour O, Stock UA, Konig K. Two-photon microscopes and in vivo multiphoton tomographs--powerful diagnostic tools for tissue engineering and drug delivery. Advanced drug delivery reviews. 2006; 58:878–896. [PubMed: 17011064]
2. Zhang EZ, Laufer JG, Pedley RB, Beard PC. In vivo high-resolution 3D photoacoustic imaging of superficial vascular anatomy. Physics in medicine and biology. 2009; 54:1035–1046. [PubMed: 19168938]
3. Kim JS, et al. Imaging of transient structures using nanosecond in situ TEM. Science. 2008; 321:1472–1475. [PubMed: 18787163]
4. Shoham D, et al. Imaging cortical dynamics at high spatial and temporal resolution with novel blue voltage-sensitive dyes. Neuron. 1999; 24:791–802. [PubMed: 10624943]
5. Hell SW. Far-field optical nanoscopy. Science. 2007; 316:1153–1158. [PubMed: 17525330]
6. DaCosta RS, Wilson BC, Marcon NE. Optical techniques for the endoscopic detection of dysplastic colonic lesions. Current opinion in gastroenterology. 2005; 21:70–79. [PubMed: 15687888]
7. Evgenov NV, Medarova Z, Dai G, Bonner-Weir S, Moore A. In vivo imaging of islet transplantation. Nature medicine. 2006; 12:144–148.
8. Piston DW. Imaging living cells and tissues by two-photon excitation microscopy. Trends Cell Biol. 1999; 9:66–69. [PubMed: 10087621]
9. Imanishi Y, Lodowski KH, Koutalos Y. Two-photon microscopy: shedding light on the chemistry of vision. Biochemistry. 2007; 46:9674–9684. [PubMed: 17676772]
10. Denk W, Strickler JH, Webb WW. Two-photon laser scanning fluorescence microscopy. Science. 1990; 248:73–76. [PubMed: 2321027]
11. Xu C, Zipfel W, Shear JB, Williams RM, Webb WW. Multiphoton fluorescence excitation: new spectral windows for biological nonlinear microscopy. Proceedings of the National Academy of Sciences of the United States of America. 1996; 93:10763–10768. [PubMed: 8855254]
12. Imanishi Y, Sun W, Maeda T, Maeda A, Palczewski K. Retinyl ester homeostasis in the adipose differentiation-related protein-deficient retina. J Biol Chem. 2008; 283:25091–25102. [PubMed: 18606814]
13. Imanishi Y, Batten ML, Piston DW, Baehr W, Palczewski K. Noninvasive two-photon imaging reveals retinyl ester storage structures in the eye. The Journal of cell biology. 2004; 164:373–383. [PubMed: 14745001]
14. Imanishi Y, Gerke V, Palczewski K. Retinosomes: new insights into intracellular managing of hydrophobic substances in lipid bodies. The Journal of cell biology. 2004; 166:447–453. [PubMed: 15314061]

15. von Lintig J, Kiser PD, Golczak M, Palczewski K. The biochemical and structural basis for trans-to-cis isomerization of retinoids in the chemistry of vision. Trends Biochem Sci. 2010; 35:400–410. [PubMed: 20188572]
16. Sparrow JR, Wu Y, Kim CY, Zhou J. Phospholipid meets all-trans-retinal: the making of RPE bisretinoids. Journal of lipid research. 2010; 51:247–261. [PubMed: 19666736]
17. Maeda A, Maeda T, Golczak M, Palczewski K. Retinopathy in mice induced by disrupted all-trans-retinal clearance. J Biol Chem. 2008; 283:26684–26693. [PubMed: 18658157]
18. Maeda A, et al. Involvement of all-trans-retinal in acute light-induced retinopathy of mice. J Biol Chem. 2009; 284:15173–15183. [PubMed: 19304658]
19. Zhou J, Jang YP, Kim SR, Sparrow JR. Complement activation by photooxidation products of A2E, a lipofuscin constituent of the retinal pigment epithelium. Proceedings of the National Academy of Sciences of the United States of America. 2006; 103:16182–16187. [PubMed: 17060630]
20. Zhou J, Kim SR, Westlund BS, Sparrow JR. Complement activation by bisretinoid constituents of RPE lipofuscin. Investigative ophthalmology & visual science. 2009; 50:1392–1399. [PubMed: 19029031]
21. Sparrow JR, et al. Involvement of oxidative mechanisms in blue-light-induced damage to A2E-laden RPE. Investigative ophthalmology & visual science. 2002; 43:1222–1227. [PubMed: 11923269]
22. Katz ML, Redmond TM. Effect of Rpe65 knockout on accumulation of lipofuscin fluorophores in the retinal pigment epithelium. Invest Ophthalmol Vis Sci. 2001; 42:3023–3030. [PubMed: 11687551]
23. Van Hooser JP, et al. Rapid restoration of visual pigment and function with oral retinoid in a mouse model of childhood blindness. Proceedings of the National Academy of Sciences of the United States of America. 2000; 97:8623–8628. [PubMed: 10869443]
24. Van Hooser JP, et al. Recovery of visual functions in a mouse model of Leber congenital amaurosis. J Biol Chem. 2002; 277:19173–19182. [PubMed: 11897783]
25. Drabent R, Bryl K, Olszewska T. A Water Environment Forces Retinyl Palmitate to Create Self-Organized Structures in Binary Solvents. Journal of Fluorescence. 1997; 7:347–355.
26. Maeda A, Golczak M, Maeda T, Palczewski K. Limited roles of Rdh8, Rdh12, and Abca4 in all-trans-retinal clearance in mouse retina. Invest Ophthalmol Vis Sci. 2009; 50:5435–5443. [PubMed: 19553623]
27. Maeda T, Maeda A, Leahy P, Saperstein DA, Palczewski K. Effects of long-term administration of 9-cis-retinyl acetate on visual function in mice. Investigative ophthalmology & visual science. 2009; 50:322–333. [PubMed: 18708622]
28. Sparrow JR, Parish CA, Hashimoto M, Nakanishi K. A2E, a lipofuscin fluorophore, in human retinal pigmented epithelial cells in culture. Investigative ophthalmology & visual science. 1999; 40:2988–2995. [PubMed: 10549662]
29. Kevany BM, Palczewski K. Phagocytosis of retinal rod and cone photoreceptors. Physiology (Bethesda). 2010; 25:8–15. [PubMed: 20134024]
30. Holz FG, et al. Progression of geographic atrophy and impact of fundus autofluorescence patterns in age-related macular degeneration. Am J Ophthalmol. 2007; 143:463–472. [PubMed: 17239336]
31. Wielgus AR, Chignell CF, Ceger P, Roberts JE. Comparison of A2E Cytotoxicity and Phototoxicity with all-trans-Retinal in Human Retinal Pigment Epithelial Cells. Photochem Photobiol. 2010
32. So PT, Dong CY, Masters BR, Berland KM. Two-photon excitation fluorescence microscopy. Annual review of biomedical engineering. 2000; 2:399–429.
33. Zipfel WR, et al. Live tissue intrinsic emission microscopy using multiphoton-excited native fluorescence and second harmonic generation. Proc Natl Acad Sci U S A. 2003; 100:7075–7080. [PubMed: 12756303]
34. Xu C, Webb WW. Measurement of two-photon excitation cross sections of molecular fluorophores with data from 690 to 1050 nm. J Opt Soc Am B. 1996; 13:481–491.
35. Maeda A, et al. Role of photoreceptor-specific retinol dehydrogenase in the retinoid cycle in vivo. J Biol Chem. 2005; 280:18822–18832. [PubMed: 15755727]

36. Batten ML, et al. Lecithin-retinol acyltransferase is essential for accumulation of all-trans-retinyl esters in the eye and in the liver. J Biol Chem. 2004; 279:10422–10432. [PubMed: 14684738]
37. Redmond TM, et al. Rpe65 is necessary for production of 11-cis-vitamin A in the retinal visual cycle. Nature genetics. 1998; 20:344–351. [PubMed: 9843205]
38. Batten ML, et al. Pharmacological and rAAV gene therapy rescue of visual functions in a blind mouse model of Leber congenital amaurosis. PLoS Med. 2005; 2:e333. [PubMed: 16250670]
39. Imanishi Y, Palczewski K. Visualization of retinoid storage and trafficking by two-photon microscopy. Methods Mol Biol. 2010; 652:247–261. [PubMed: 20552433]
40. Maiti S, Shear JB, Williams RM, Zipfel WR, Webb WW. Measuring serotonin distribution in live cells with three-photon excitation. Science. 1997; 275:530–532. [PubMed: 8999797]

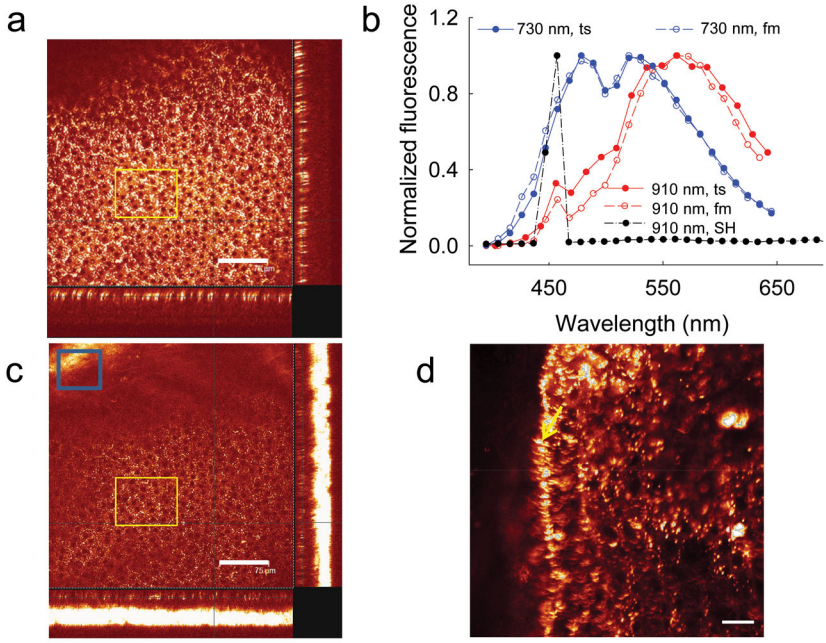

Figure 1. Multi–photon excitation of a 6–month–old wild type (WT) mouse eye at 730 and 910 nm produced emission spectra indicating more than one fluorophore

(**a**) A series of TPM images of an intact mouse eye were obtained along the axis perpendicular to the RPE layer with an excitation wavelength of 730 nm. The main box reveals the enface image of RPE cells; the two cross–section images, one shown at the bottom and the other at the right edge, were assembled from a series of z-slice images. The yellow outlined rectangle represents the region from which fluorescence was collected for spectral analysis with the excitation light focused on the RPE. Scale bar, 75 μm. (**b**) Fluorescence emission spectra from the RPE of an intact mouse eye through the sclera (ts) and from flat–mounted (fm) mouse RPE are super–imposable. The second harmonic signal (SH) exhibits a sharp maximum at half of the 910 nm excitation wavelength. (**c**) A series of TPM images of an intact mouse eye obtained with an excitation wavelength of 910 nm. In the region of the blue outlined rectangle, a strong second harmonic signal from the sclera was dominant, as the curvature of the eye brought the sclera more into focus. Scale bar, 75 μm. The yellow outlined rectangle represents the region from which fluorescence was collected for spectral analysis shown in **b**. (**d**) TPM image of flat–mounted *ex vivo* RPE. Part of the RPE is folded over, exposing a sagittal view of retinosomes, indicated with the yellow arrow. Scale bar, 20 μm.

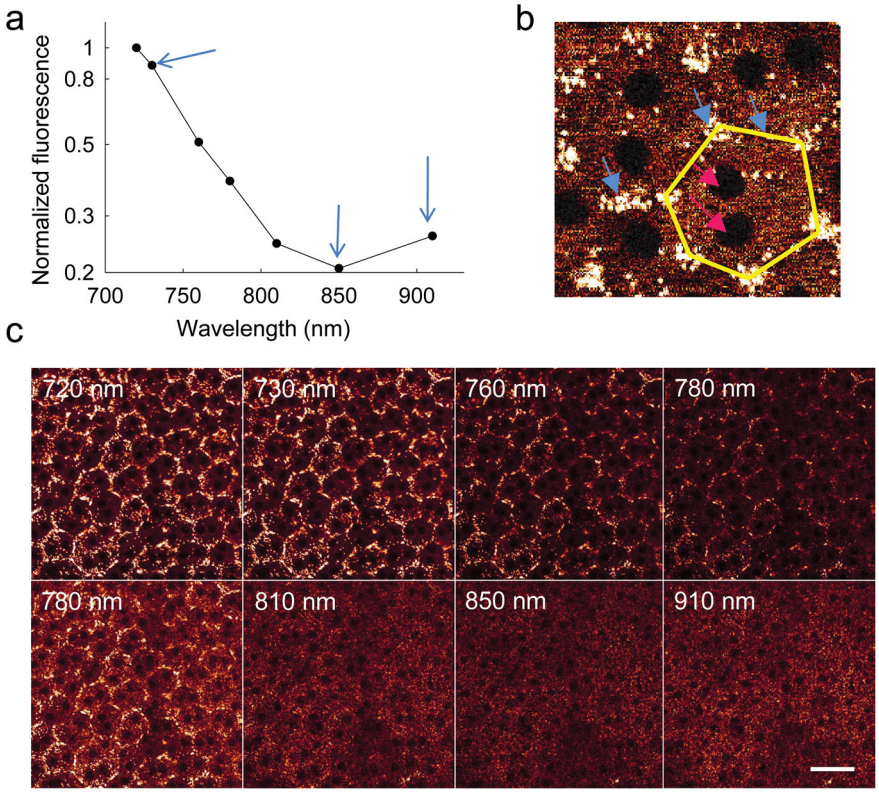

Figure 2. Multi–photon excitation of the RPE in an intact 6–month–old WT mouse eye at different wavelengths of excitation light

(**a**) Graph showing fluorescence as a function of excitation light wavelength. Fluorescence intensities were obtained as mean pixel values from the area covered by at least 20 RPE cells in focus and were normalized to the maximum value at 720 nm. Blue arrows (from left to right) indicate fluorescence in response to 730, 850 and 910 nm excitation. (**b**) Zoomed–in two–photon image of RPE cells obtained with 730 nm excitation. Blue arrows denote retinosomes (white) clustering along plasma membranes; edges of one RPE cell are highlighted in yellow. Dark, mostly double nuclei are indicated by pink arrows. (**c**) Images of RPE cells at different excitation wavelengths indicated in each panel. All images were obtained with 10 mW of laser power. Photomultiplier tube (PMT) gain and offset were kept constant for images in the top row. Then the gain was readjusted and kept constant for the images in the bottom row. Scale bar, 38 μm.

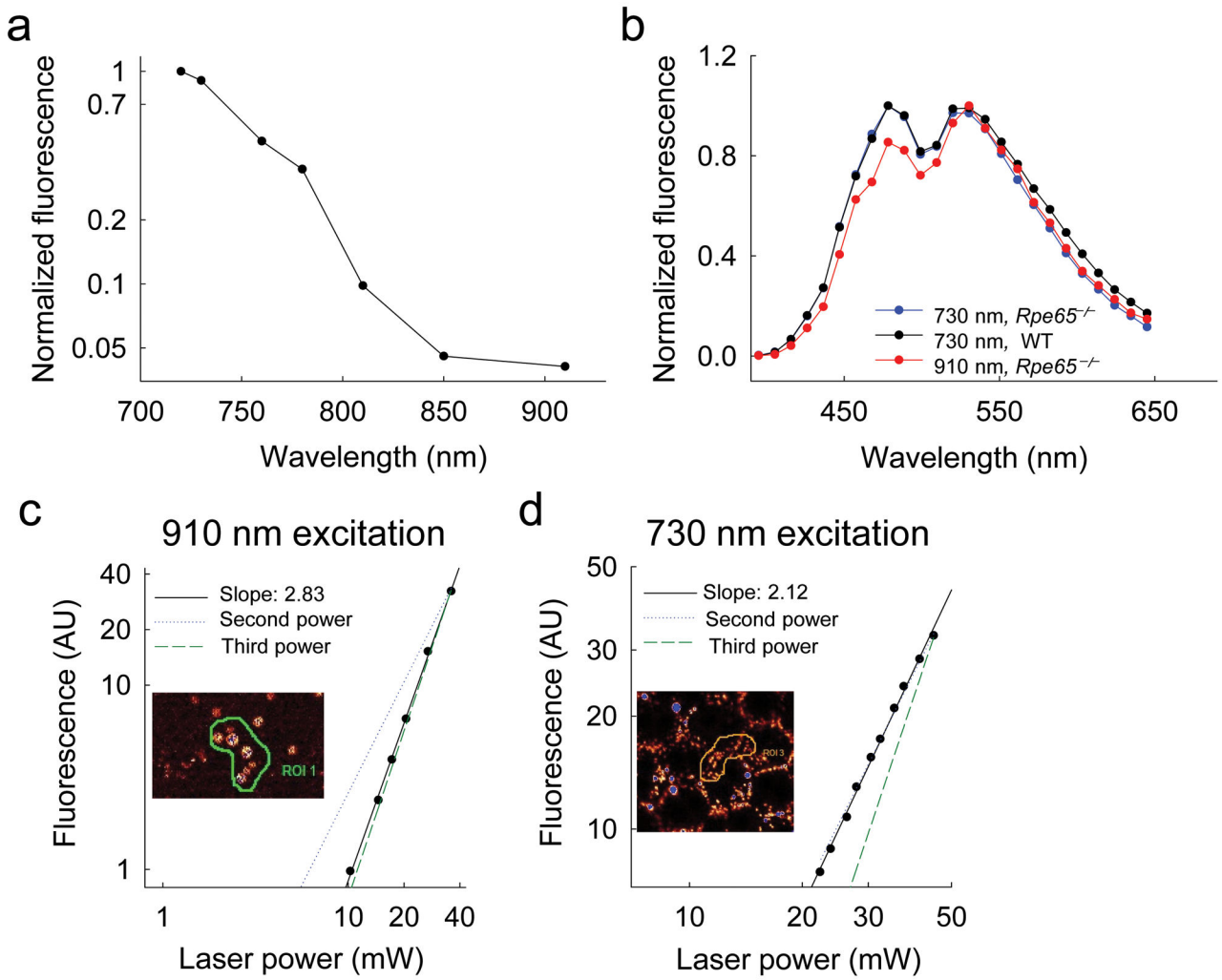

Figure 3. Visualization of retinosomes by three–photon excitation spectroscopy in the intact 7–week–old *Rpe65*$^{-/-}$ mouse eye

(**a**) Graph showing fluorescence intensity as a function of excitation light wavelength; fluorescence intensity was calculated as a mean pixel value from the area covered by at least 20 RPE cells in focus during imaging and normalized to the maximum value at 720 nm excitation. (**b**) Emission spectra from the RPE of WT and *Rpe65*$^{-/-}$ mouse eyes excited with laser light at 730 nm and 910 nm. (**c**) Logarithmic plot of fluorescence intensity as a function of excitation power shows evidence of three–photon excitation at an excitation wavelength of 910 nm. The mean pixel value was proportional to the 2.83rd power. (**d**) At an excitation wavelength of 730 nm, the mean pixel value was proportional to the 2.12th power of the laser power. In (**c**) and (**d**) data points are shown as black circles. Modeling of the pure second power dependence is shown by the blue dotted line and modeling of the third power dependence is indicated by the green dashed line. *Insets* depict areas containing retinosomes from which fluorescence was quantified.

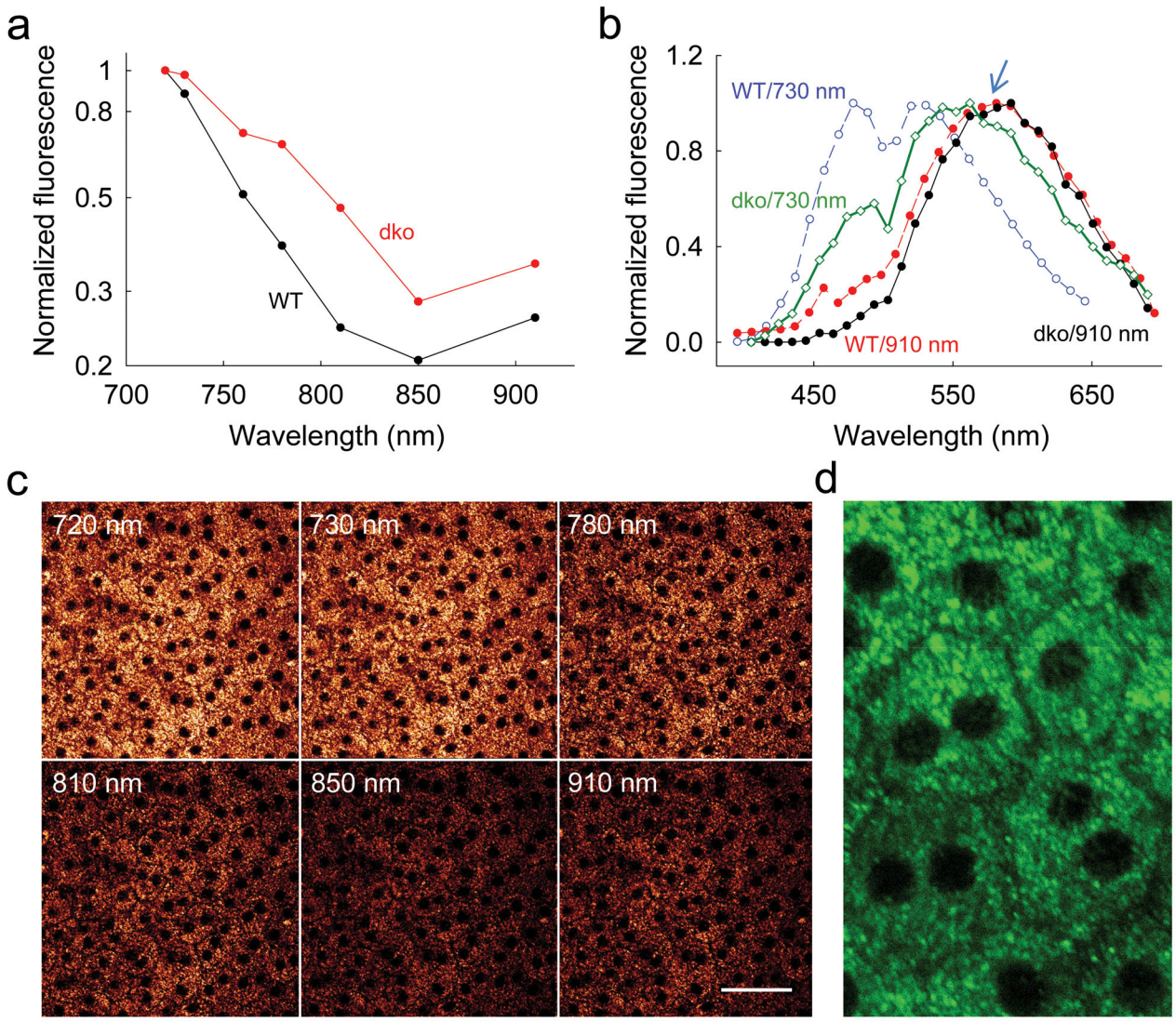

Figure 4. Two–photon excitation of 6–week–old *Abca4*$^{-/-}$*Rdh8*$^{-/-}$ (dko) intact mouse eye

(**a**) Fluorescence intensity as a function of excitation wavelength, normalized to maximum emission at 720 nm excitation. (**b**) Emission spectra from RPE of WT and dko mice excited with laser light at 730 nm and 910 nm. Blue arrow points to 580 nm. (**C**) Images of dko mouse RPE at different excitation wavelengths. All images were obtained with 10 mW of laser power; PMT gain and offset were kept constant. Scale bar 50 μm. (**d**) Zoomed–in TPM image of unstained dko mouse RPE. Fluorescent granules are distributed uniformly throughout cells with clearly visible boundaries. Green color was arbitrarily chosen to make the image details more visible. Scale bar 25 μm.

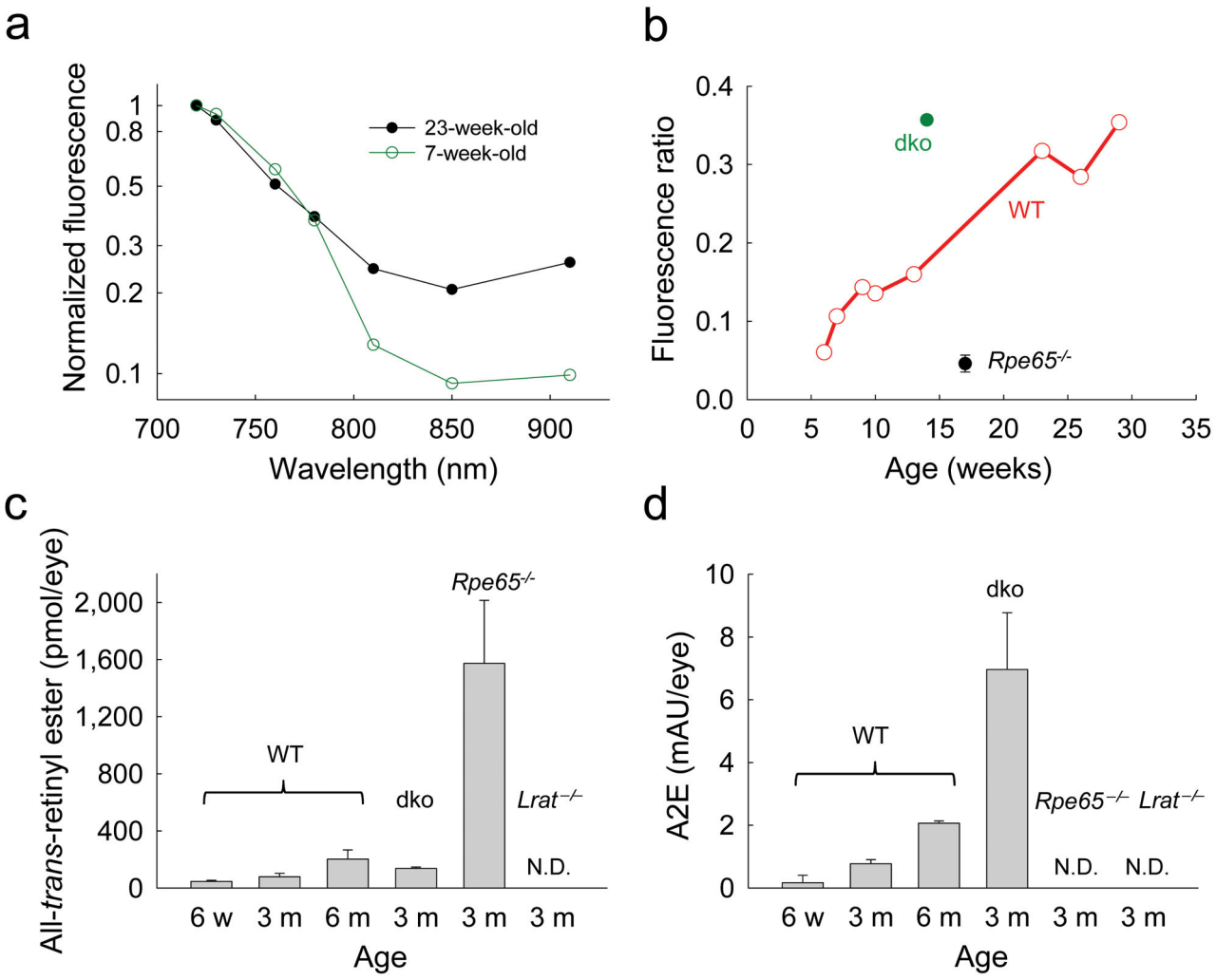

Figure 5. Age–dependent changes in fluorophore accumulation in mouse eyes

(**a**) Two–photon excitation fluorescence intensity of WT mouse retina drops with increasing wavelengths of light excitation; the decline of fluorescence emission is more rapid in younger than in older mice. Fluorescence emission values were normalized to that observed with 720 nm excitation. (**b**) Ratios of fluorescence excited with 910 nm light relative to fluorescence excited with 730 nm light increased with age in WT mice. *Abca4*$^{-/-}$*Rdh8*$^{-/-}$ (*dko*) mice displayed higher fluorescence ratio than WT mice. (**c**) Increasing levels of all–*trans*–retinyl esters determined by normal phase HPLC were found in the eyes of WT mice at the ages of six weeks, three months and six to seven months. *Rpe65*$^{-/-}$ mouse eyes exhibited more than a 15–fold increase in all–*trans*–retinyl ester accumulation as compared to age–matched WT mouse eyes. No all–*trans*–retinyl esters were detected in *Lrat*$^{-/-}$ mouse eyes (n=5 for each group). (**d**) A2E was extracted from mouse eyes and quantified by reverse phase HPLC. Control WT mice were evaluated at six weeks, three months and six to seven months of age and exhibited increased A2E amounts in an age–dependent manner. A2E levels in 3–month–old *Abca4*$^{-/-}$*Rdh8*$^{-/-}$ mouse eyes were markedly higher than in age–matched and older WT controls. No A2E was detected in the eyes of 3–month–old

Rpe65$^{-/-}$ and *Lrat*$^{-/-}$ mice (n=5 for each group). In (**c**) and (**d**) data columns are shown with one standard deviation bars.